A top-down evaluation of bottom-up estimates to reduce uncertainty in methane emissions from Arctic wetlands

Luana S. Basso[1], Goran Georgievski[2,3], Victor Brovkin[2], Christian Beer[4], Christian Rödenbeck[1], Mathias Göckede[1]

[1]Department of Biogeochemical Signals, Max Planck Institute for Biogeochemistry, Jena, 07745, Germany
[2]Department of Climate Dynamics, Max Planck Institute for Meteorology, Hamburg, 20146, Germany
[3]Earth Resilience Science Unit, Potsdam Institute for Climate Impact Research, Germany
[4]Department of Earth System Sciences, University of Hamburg, Hamburg, 20146, Germany

Correspondence to: Luana S. Basso (lbasso@bgc-jena.mpg.de)

Abstract.

Wetlands are a major natural source of atmospheric CH_4, however, accurately estimating their emissions is difficult due to the complex biogeochemical interactions and spatial heterogeneity of wetland environments. This study explores how a combination of atmospheric inverse and process-based modelling can reduce the discrepancy in Arctic wetland estimates between bottom-up and top-down approaches. We employed the Jena CarboScope global inversion system, incorporating prior wetland fluxes simulated by the JSBACH land surface model, which is part of the Max Planck Institute Earth System Model (MPI-ESM). We conducted a series of inversion experiments, each incorporating JSBACH-generated CH_4 fluxes based on different CH_4 production Q_{10} values, which represents the temperature dependence of CH_4 production. Additionally, we examined the impact of changing the baseline f_{CH_4} fraction value, which defines the fraction of anaerobically mineralized carbon converted to CH_4, while keeping all other JSBACH and inversion settings constant. Our findings show that, at a pan-Arctic scale, using a CH_4 Q_{10} value of 1.8 produces the best agreement between the two approaches. However, no single Q_{10} value yielded optimal agreement between the simulated fluxes and the fluxes inferred from atmospheric observations across all subregions. Instead, the best performance varied spatially, with different CH_4 production Q_{10} values and baseline f_{CH_4} fraction leading to a better flux agreement in specific areas. These results highlight the importance of using regionally specific parameters to more accurately estimate wetland CH_4 emissions, and the potential of employing atmospheric inversions to guide bottom-up process models towards regionally representative parameter settings.

1. Introduction

Methane (CH_4) is the second most important anthropogenic greenhouse gas and it is emitted from both natural and anthropogenic sources. Combined wetlands and inland freshwaters are the largest natural source of CH_4 to the atmosphere, accounting for about 28-37% (by bottom-up and top-down estimates, respectively) of the global total CH_4 emissions (Saunois et al., 2025). However, quantifying these emissions remains challenging due to the complexity of biogeochemical processes

and the spatial variability of these ecosystems. Constraining CH_4 budgets is particularly relevant in the Arctic-Boreal region, which is warming faster than most other regions (Rantanen et al., 2022), and at the same time contains extensive wetlands and permafrost landscapes storing significant amounts of soil carbon (Hugelius et al., 2024). Under warming conditions, this carbon can be mobilized and potentially release substantial amounts of CH_4 into the atmosphere. Large uncertainties in Arctic CH_4 emission estimates limit our ability to quantify the region's contribution to the global CH_4 budget and its climate feedbacks.

Global and regional CH_4 emissions are estimated using both bottom-up or top-down approaches. Bottom-up methods, including inventories, data-driven ecosystem flux upscaling and process-based models, provide detailed information with fine-scale resolution for both, processes and spatial heterogeneity. Process-based models simulate CH_4 emissions by mathematically representing ecosystem dynamics, biogeochemical cycles, and physical processes. However, extrapolating these estimates to regional or global scales is challenging due to the strong spatial variability in wetland characteristics (e.g., extent, hydrology and vegetation), as well as sensitivity of the models to parameterizations. Top-down approaches estimate net surface-atmosphere CH_4 fluxes using atmospheric observations (in situ, flask and/or satellite measurements) in combination with prior flux information (from process-based models and/or inventories), and atmospheric transport and chemistry models to link surface sources with atmospheric observations. Their ability to provide accurate estimates of net surface-atmosphere fluxes is limited by sparse observational coverage, particularly in remote regions, as well as by uncertainties in atmospheric transport, prior flux estimates, and atmospheric CH_4 sink processes (Houweling et al., 2017). These limitations can lead to significant uncertainties in the magnitude and spatial distribution of inferred emissions, which makes attributing fluxes to specific sources or processes challenging. Still, despite these limitations, the inverse modeling approach allowed us to derive important constraints on the global sources and sinks of CH_4 (Houweling et al., 2017).

Although both approaches are widely used, substantial discrepancies exist between bottom-up and top-down estimates of CH_4 emissions. From 2010 to 2019, top-down approaches estimated global CH_4 emissions at 575 $TgCH_4\ y^{-1}$ (553-586 $TgCH_4\ y^{-1}$), whereas bottom-up estimates were approximately 15% higher, at 669 $TgCH_4\ y^{-1}$ (512-849 $TgCH_4\ y^{-1}$) (Saunois et al., 2025). Similar differences are evident in the high-northern latitudes regions, where wetlands and inland waters dominate emissions. In the Arctic-Boreal region, bottom-up estimates of 50 $TgCH_4\ y^{-1}$ (29-71 $TgCH_4\ y^{-1}$) contrast with top-down estimates of 20 $TgCH_4\ y^{-1}$ (15-24 $TgCH_4\ y^{-1}$) (Hugelius et al., 2024).

Mechanistic modeling of net surface CH_4 emissions requires capturing a range of complex, interacting processes (Conrad, 1999; Moser et al., 2026; Riley et al., 2011). As a key parameter, the net CH_4:CO_2 production ratio is determined by the relative importance of several biogeochemical processes, which in turn are dependent on environmental conditions, and a large range of this production ratio has been observed (Knoblauch et al., 2018). As a consequence, global-scale land surface models often represent anaerobic CH_4 production in a simplified way, i.e. as a first-order decay of soil organic matter with adjusted rate constants, applying a fixed ratio of CH_4 versus CO_2 production (Guimberteau et al., 2018; Kleinen et al., 2020; Moser et al., 2026; Ricciuto et al., 2021; Sellar et al., 2019). Here, the models can differ in whether the ratio applies to the CH_4 production or emission.

Biogeochemical process models require balancing the inclusion of key mechanisms with limitations such as structural and parameter uncertainty, spatial heterogeneity, sparse observational data, uncertain initial and boundary conditions, and computational constraints (Riley et al., 2011). Regarding the simulation of CH_4 emissions, a higher CH_4:CO_2 ratio indicates a greater dominance of CH_4 in production and emission relative to CO_2 (Chinta et al., 2024), while a higher CH_4 production Q_{10} indicates that CH_4 production increases more rapidly with rising temperatures. As regional model sensitivity varies and site-specific measurements may not be representative across broader areas, both the CH_4:CO_2 ratio and the CH_4 production Q_{10} are uncertain at large spatial scales. For example, increasing CH_4 production Q_{10} in high-latitude regions can reduce simulated CH_4 emissions by more than half, because the temperature-dependent component, scaled relative to a reference temperature of 295 K, leads to a decline in CH_4 production rate at the lower temperatures typical of these regions (Riley et al., 2011). As many large-scale land surface models still rely on simplified, fixed CH_4 production fractions, their ability to accurately represent observed spatiotemporal variability in CH_4:CO_2 production ratios across Arctic landscapes is therefore limited (Moser et al., 2026). These differences in model structure, parameterization and initialization contribute strongly to relative high uncertainties in wetland estimates (Poulter et al., 2017).

The JSBACH v3.2 model (Reick et al., 2021) that we apply in this study is taking the first approach and mechanistically distinguish between methanogenesis and methanotrophy. In JSBACH v3.2, anaerobic decomposition and CH_4 oxidation are temperature dependent and the CH_4:CO_2 production ratio is also assumed to follow a Q_{10} temperature sensitivity (Kleinen et al., 2020). This formulation allows the relative importance of the above-mentioned underlying biogeochemical processes changes in space and time depending on the soil temperature. In addition, making the CH_4:CO_2 production ratio temperature dependent allows us to additionally tune CH_4 versus CO_2 production across bioclimatic zones. Still, the optimum parameter setting of the Q_{10} value for this temperature dependency of the CH_4:CO_2 production ratio is still highly uncertain.

This study therefore explores novel concepts for using atmospheric inverse modeling to constrain parameter settings in bottom-up estimates of wetland CH_4 emissions in the Arctic-Boreal region. Using the Jena CarboScope global inversion system, we employed prior fluxes from the JSBACH land surface model (a component of the MPI Earth System Model) and systematically varied key parameters that govern CH_4 production. Specifically, we tested a range of Q_{10} values, which define the temperature sensitivity of CH_4 production, and different f_{CH_4} baseline values, which determine the proportion of anaerobically mineralized carbon converted to CH_4. However, a portion of the produced CH_4 is oxidized to CO_2. Since transport pathways determine how much CH_4 is exposed to oxidation on its way to the surface, they reduce the resulting CH_4:CO_2 emission ratio. We kept other model settings constant throughout these tests. Integrating these parameter sensitivity experiments into the inversion framework allowed us to assess which parameterizations yield the most consistent fluxes with atmospheric observations. This approach enables us to identify regionally representative parameter settings and guide parameterizations that could improve the consistency between bottom-up process models and top-down constraints on Arctic-Boreal wetland CH_4 emissions.

2. Methods

2.1. Region and time period of interest

Our Arctic-Boreal domain was defined based on The Boreal-Arctic Wetland and Lake Dataset – BAWLD (Olefeldt et al., 2021), and we divided this region into 6 sub-regions for more detailed spatial analyses (Alaska, western Canada, eastern Canada, Europe including Greenland, western Russia, eastern Russia, Fig. 1). In recent decades, the atmospheric observation network suitable for inverse modeling has expanded across the Arctic, with a considerable increase in available sites after 2010 (Vogt et al., 2025). However, due to data-sharing disruptions associated with the ongoing conflict involving Russia and Ukraine, observational data from Russian stations has been limited since 2022. Consequently, this study focuses on the period from 2010 to 2021, when data coverage from surface stations was more consistent across the full domain.

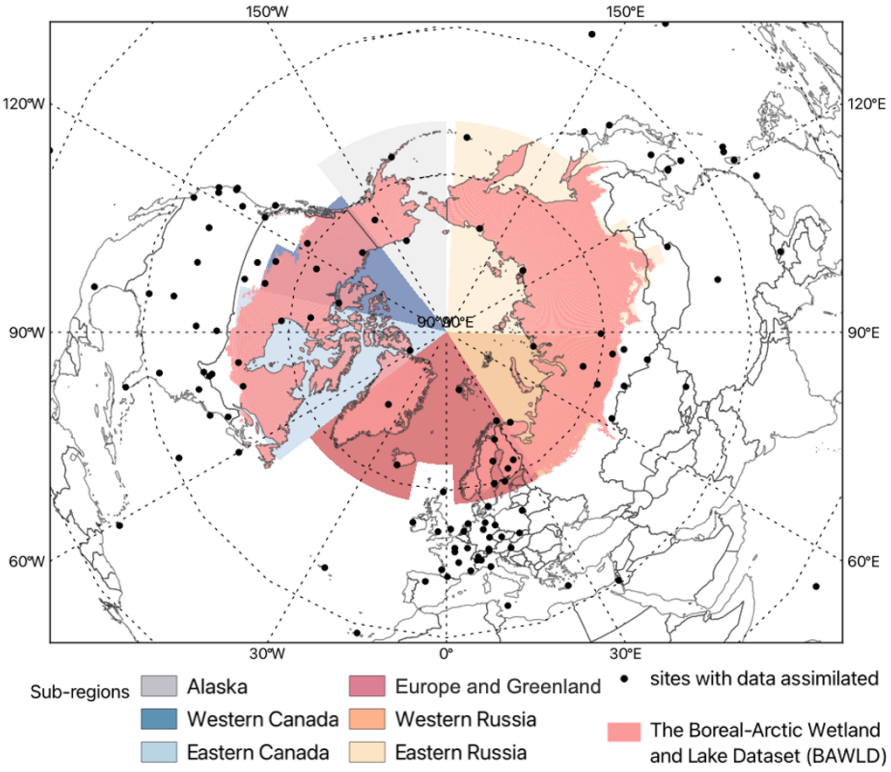

Figure 1: Geographic distribution of surface sites operated by different network providers where flask-based and/or continuous in-situ CH_4 measurements are available for assimilation into the inverse model (black dots; Supplementary Table 1). The colored boxes delineate the Arctic-Boreal regions (Alaska, western Canada, eastern Canada, Europe including Greenland, western Russia, eastern Russia), as defined based on The Boreal-Arctic Wetland and Lake Dataset (BAWLD) (Olefeldt et al., 2021).

2.2. Wetland estimates used as prior fluxes in the inverse modelling

In this study, we utilize the JSBACH model (Reick et al., 2021), the land component of the MPI-ESM (Mauritsen et al., 2019), to estimate bottom-up wetland CH_4 emissions. JSBACH is run in standalone mode at T63 resolution (approximately 1.85°, or 185 km) and driven by CRUJRA2.3 (Harris, 2019) climate forcing. Soil hydrology and thermodynamics follow the multilayer formulation of Hagemann and Stacke (2015), with permafrost-related processes implemented as described by Ekici et al. (2014). Soil organic carbon (SOC) decomposition is simulated as a first-order decay process that depends on surface air temperature, water availability, and litter size, following the YASSO model formulation (Tuomi et al., 2011) and its implementation in JSBACH by Goll et al. (2015).

The wetland area fraction of the grid is determined using TOPMODEL (Beven and Kirkby, 1979), a conceptual rainfall-runoff model that estimates inundation based on the compound topographic index (CTI). If the inundated fraction of the grid is non-frozen (depending on the soil temperature), it is considered a CH_4-emitting area. The methodology for wetland CH_4 production and transport is adopted from Riley et al. (2011), and the details of the TOPMODEL and its implementation for wetland CH_4 within JSBACH are outlined in Kleinen et al. (2020).

Methane production and the transport pathways that move CH_4 to the surface (diffusion, plant-mediated aerenchyma and ebullition) follow the scheme of Riley et al. (2011), as implemented in JSBACH by Kleinen et al. (2020). Under anaerobic conditions, a proportion of SOC (f_{CH_4}) is converted to CH_4, while the remaining is converted to CO_2. The temperature dependence of f_{CH_4} is represented using a Q_{10} formulation.

$$f_{CH_4} = f_{CH_4,baseline} \cdot Q_{10}^{(T_{soil}-295)/10K} \qquad \text{Equation 1}$$

Oxidation reduces the amount of CH_4 that reaches the atmosphere. Consequently, the net CH_4:CO_2 emission ratio depends on production and oxidation rates, as well as transport pathways, which control the amount of CH_4 exposed to oxidation. A simplified conceptual relationship is as follows:

$$CH_4 : CO_2 = \frac{f_{CH_4} P - O_{CH_4}}{(1-f_{CH_4})P + O_{CH_4}} \qquad \text{Equation 2}$$

where P is gross anaerobic SOC decomposition and O is the amount of CH_4 oxidized before emission.

To evaluate how sensitive CH_4 wetland emission estimates are to key parameters, we conducted nine experiments in which we varied only the Q_{10} coefficient for CH_4 production and the baseline f_{CH_4} fraction (Fig. 2b). Specifically, we tested three different Q_{10} values ranging from 1.4 to 2.2, consistent with commonly used values reported in literature review (Moser et al., 2026), and baseline f_{CH_4} fractions from 0.33 to 0.38. These combinations are summarized in Table 1 and were chosen to identify parameter sets that best align with the observed atmospheric data. All other carbon decomposition, hydrological, transport, and oxidation processes follow the standard JSBACH configuration.

2.3. Inverse modeling setup

We used the Jena CarboScope Inversion System (Rödenbeck, 2005) to quantify CH_4 emissions between the surface and the atmosphere globally from 2010 to 2021, with the evaluation and interpretation of fluxes focused on the Arctic-Boreal region. This is a linear Bayesian framework that infers surface-atmosphere CH_4 fluxes by combining prior flux estimates with atmospheric CH_4 mole fraction measurements and accounting for their respective uncertainties. The flux vector f represents the net flux per grid cell per time step. The Jena CarboScope enables f to be represented as the sum of different flux components, each of which is modelled independently using its own statistical linear flux model. These independent a priori error covariance structures allow deviations from the prior flux estimate to be attributed to specific components during the inversion process. In this study, the a priori shape uncertainty was defined as 100% of the prior flux for each flux category. All flux categories were optimized, assuming spatial correlation lengths of ~500 km and temporal correlation lengths of about 15 days. Temporal and spatial fluxes are optimized within a Bayesian inversion framework that minimizes a cost function combining prior and observational constraints. The solution is obtained analytically using the linear Bayesian approach, which yields maximum posterior flux estimates and their associated uncertainties. Details of the cost function formulation and solution method can be found in the CarboScope technical report (Rödenbeck, 2005).

A total of 154 stations were assimilated for the global domain (Fig.1; Supplementary Table 1). These CH_4 observations were obtained from multiple global and regional networks (ICOS RI et al., 2024; Panov et al., 2021; Sasakawa et al., 2010, 2025; Schuldt et al., 2023), with the majority of sites located in the Northern Hemisphere, including 33 stations within the Arctic-Boreal domain. Most observational data used in this study were accessed through NOAA GML ObsPack (Schuldt et al., 2023), ICOS Carbon Portal (ICOS RI et al., 2024), World Data Centre for Greenhouse Gases (WDCGG) database (https://doi.org/10.50849/WDCGG_CH4_ALL_2023), and JR-STATION network (Sasakawa et al., 2010, 2025); further details are provided in the "Data Availability section". Detailed information on the stations with assimilated data is given in Supplementary Table 1. For tower sites with multiple intake heights available, we assimilated only data from the highest height in the inversion, and for the continuous data, we use only daytime measurements. The transport model used in CarboScope is the TM3 global atmospheric tracer model, an Eulerian transport model that solves the continuity equation (and parameterizations of boundary layer and convective mixing) for atmospheric tracers in a three-dimensional grid over the globe (Heimann and Körner, 2003). The model has a spatial resolution of approximately 3.8° latitude by 5° longitude, with 19 vertical layers, and it is driven by meteorological inputs from the NCEP reanalysis dataset (Kalnay et al., 1996). Flux inversions were conducted at the TM3 spatial resolution and a daily temporal resolution. Since the model is initialized with a homogeneous background concentration of methane, it is run for at least one year before to the period of interest to avoid any impact resulting from the model spin-up. To account for model-data mismatch, including the representation error of the measurements within the transport model, each station is assigned a weekly error value based on how well the atmospheric transport model can capture local atmospheric dynamics. For example, for mountain sites and stations near shores samples are assigned a smaller error of 15 ppb, whereas surface sites in regions with complex circulation patterns receive a larger error of 30 ppb. Additionally,

to ensure balanced representation across observational sites, particularly between continuous and sparse time series, we applied a data density weighting scheme, assigning equal influence to each weekly period, regardless of data frequency. Without this adjustment, sites with high-frequency data would dominate the cost function solely because of the greater number of observations. To avoid this, the uncertainty of each measurement is multiplied by the number of observations per week. This corresponds to the assumption that errors are correlated on weekly timescales, meaning that one week of hourly data provides roughly the same amount of independent information as one weekly flask sample (Rödenbeck, 2005).

Prior CH_4 flux estimates include five source categories, all of which were optimized: wetlands, other natural sources, anthropogenic, ocean and fire emissions. The monthly mean emissions from wetlands and fires were obtained from the JSBACH model (Kleinen et al., 2020), as previously described. Fire emissions represent the simulated biomass burning emissions of JSBACH and were prescribed as monthly varying prior fluxes. Additional natural sources, such as termites and wild animal emissions taken from JSBACH (Kleinen et al., 2020) and geological emissions from Etiope et al. (2019) were combined as the "other natural source" category. Emissions from oceans were obtained from Weber et al. (2019) and implemented as a non-seasonal climatology. Anthropogenic emissions were obtained from the EDGAR inventories database (https://edgar.jrc.ec.europa.eu) version 8 (Crippa et al., 2023) and are provided as monthly global fluxes. This category includes emissions from agriculture, livestock, waste management, fossil fuel exploitation and other minor anthropogenic sources except biomass burning. Emissions of CH_4 from inland water (freshwater) were not included as a separate prior category and are therefore not explicitly optimized in the inversion framework.

CH_4 chemical loss includes loss due to OH and Cl in the troposphere, as well as OH, Cl, and $O(^1D)$ in the stratosphere. For tropospheric OH, we use the monthly three-dimensional OH fields calculated by Spivakovsky et al. (2000), which are based on observed climatological distributions of OH precursors and scaled to match the observed CH_3CCl_3 lifetime. The monthly climatological loss rates of CH_4 in the stratosphere due to OH, Cl, and $O(^1D)$ were derived from a simulation of the ECHAM5/MESSy1 chemistry transport model (Jöckel et al., 2006). Additionally, tropospheric Cl loss is simulated using a recent model-derived estimate of tropospheric Cl (Hossaini et al., 2016). The surface sink from upland soils and the ocean was implemented as a zeroth-order reaction with prescribed reaction rates that occur only in the surface-most model layer. Reaction rates for the microbial oxidation of atmospheric CH_4 in soil were based on the uptake estimates from the LPJ-Bern model (Spahni et al., 2011).

2.4. Evaluating Bottom-Up Emissions Using Top-Down Constraints

Previous studies have used atmospheric inversion models to evaluate different bottom-up estimates and determine which one best reproduces observed atmospheric CH_4 data (Kim et al., 2011; Miller et al., 2016), providing an effective framework for model evaluation. In this study, we evaluated the performance of different JSBACH parameterizations by using the CH_4 wetland emission outputs from each experiment as wetland prior fluxes in a top-down atmospheric inversion framework. The inversion then generated posterior fluxes, reflecting the adjustments needed to align the prior emissions with atmospheric CH_4

observations. These adjustments take into account uncertainties in atmospheric transport, observational errors, and model representation. In this study, we used the model adjustment defined as the difference between posterior and prior fluxes, calculated as the mean monthly and mean annual values across the Arctic-Boreal region from 2010 to 2021. First, we identified the parameterization resulting in the lowest mean model adjustment across the entire domain.

For the monthly analysis, we first computed the mean monthly prior flux and the mean monthly posterior flux, and then defined the model adjustment as the difference between these two means. For the annual analysis, we calculated the mean annual prior and posterior fluxes and again defined the adjustment as their difference. This allowed us to determine which JSBACH configuration provided the best overall agreement with atmospheric constraints at the pan-regional scale and investigate temporal variability.

Next, we examined spatial variability of the difference between posterior and prior fluxes using different JSBACH parameterizations as wetland priors. At the grid-cell level, we identified the parameter combination that minimized annual model adjustment, thereby providing the best match to the top-down atmospheric constraints. To conduct this analysis, an ensemble of posterior fluxes was calculated based on each CH_4 production Q_{10} value from the prior wetland flux. This approach was supported by the observation that CH_4 production Q_{10} significantly influenced CH_4 emission estimates compared to the baseline f_{CH_4} fraction. Additionally, posterior fluxes from priors with different baseline f_{CH_4} fraction scenarios remained highly similar for a given Q_{10} value. As a result, maps were created by calculating the absolute difference between the posterior ensemble of the respectively Q_{10} value and prior CH_4 fluxes for each experiment at each grid-cell. Then, the annual mean adjustment was calculated and we identified the parameterization that resulted in the smallest adjustment at each grid-cell. In summary, each grid-cell shows the experiment that best matched the atmospheric CH_4 observations.

3. Results and Discussion

3.1 Sensitivity of JSBACH CH_4 wetland emission estimates to CH_4 production Q_{10} and baseline f_{CH_4} fraction in the Arctic–Boreal region

Table 1 summarizes the experiments and parameters combinations that have been tested in the JSBACH model and used as a wetland prior in the atmospheric inversions. Across the Arctic-Boreal region, our nine experiments produced annual mean CH_4 wetland estimates ranging from 13.8 to 33.5 $TgCH_4\ y^{-1}$. These estimates are consistent with previously published bottom-up estimates of ~15-50 $TgCH_4\ y^{-1}$, with most studies reporting mean values near 20-25 $TgCH_4\ y^{-1}$ (Christensen et al., 1996; Ying et al., 2025; Yuan et al., 2024; Zhang et al., 2025). It should be noted that these studies consider different spatial domains and time periods. The estimates obtained using a Q_{10} value of 1.8 align most closely with this published range among our experiments.

Table 1. Summary of JSBACH wetland CH_4 estimates used as prior fluxes in the inversions and posterior fluxes estimates for each respective model run.

JSBACH parameterization		Arctic-Boreal annual mean CH_4 emission ($TgCH_4\ y^{-1}$)*		
Baseline f_{CH_4} fraction	Q_{10} model	JSBACH estimates (prior)	Posterior estimates	Mean model adjustment
0.33	1.4	31.7 ± 1.1	25.0 ± 1.4	-6.7
0.33	1.8	20.0 ± 0.7	22.9 ± 1.1	2.9
0.33	2.2	14.6 ± 0.5	21.2 ± 0.9	6.6
0.35	1.4	29.7 ± 0.9	24.8 ± 1.5	-5.0
0.35	1.8	18.9 ± 0.6	22.7 ± 1.1	3.8
0.35	2.2	13.8 ± 0.5	20.9 ± 0.9	7.1
0.38	1.4	33.5 ± 1.0	25.2 ± 1.6	-8.2
0.38	1.8	21.3 ± 0.7	23.3 ± 1.2	2.0
0.38	2.2	15.5 ± 0.5	21.6 ± 1.0	6.1

*The annual mean between 2010 and 2021, with the standard deviation representing interannual variability.

Emissions peaked during the summer months (July-August), with a mean emission ranging from 6.8 to 15.5 $TgCH_4\ y^{-1}$ (Fig. 2b). These larger emissions were followed by spring (May-June; range of 3.5-7.8 $TgCH_4\ y^{-1}$), autumn (September-October; range of 2.8-7.7 $TgCH_4\ y^{-1}$), and winter with the lower emissions (November-April; range of 0.7-2.7 $TgCH_4\ y^{-1}$). The timing of the peak in wetland emissions aligns with previous bottom-up estimates (Ying et al., 2025). At the sub-regional scale, emissions showed substantial spatial variability (Fig. 2c). The highest annual mean fluxes were found in western Russia (3.4-8.7 $TgCH_4\ y^{-1}$, depending on the parameter set), followed by eastern Canada (3.4-8.2 $TgCH_4\ y^{-1}$), eastern Russia (3.1-7.2 $TgCH_4\ y^{-1}$), western Canada (1.8-4.4 $TgCH_4\ y^{-1}$), Europe including Greenland (1.5-3.4 $TgCH_4\ y^{-1}$), and Alaska (0.5-1.6 $TgCH_4\ y^{-1}$).

In general, increasing the baseline value of the f_{CH_4} fraction from 0.33 to 0.38 increases CH_4 production. However, an increase in the CH_4 production Q_{10} parameter decreases CH_4 production for temperatures below 295 K (the reference temperature) and increases it for temperatures higher than 295 K. This means that increasing Q_{10} values from 1.4 to 2.2 reduces wetland CH_4 emissions in the comparatively cold Arctic region (Table 1 and Fig. 2). The sensitivity of wetland CH_4 to the Q_{10} temperature response and the baseline f_{CH_4} fraction is evident when comparing seasonal cycles over the Arctic-Boreal domain (Fig. 2b). For example, contrasting the simulations with baseline f_{CH_4} fraction equaling 0.33 and varying CH_4 production Q_{10} values (from 1.4 to 2.2), shows that increasing Q_{10} significantly reduces annual wetland mean CH_4 emission in this region by ~ 54% (~17 $TgCH_4\ y^{-1}$). This reduction is not uniform throughout the year. Although winter emissions are relatively low, increasing Q_{10} from 1.4 to 2.2 results in a ~70% decrease compared to a ~50-59% decrease during the summer, spring and fall. Similarly, the influence of the baseline f_{CH_4} fraction can be observed by keeping Q_{10} constant, for example at 1.4, and varying

the baseline f_{CH_4} fraction from 0.33 to 0.38. This increase leads to an increase of up to 6% in the annual wetland CH_4 emissions for the region. In general, our parameter sensitivity tests show that CH_4 production Q_{10} has a stronger effect on emission variability than the baseline f_{CH_4} fraction. These wetland CH_4 emission estimates with different parameterizations were subsequently integrated into the Jena CarboScope atmospheric inversion framework as wetland prior fluxes to determine the combination that closest align with atmospheric CH_4 observations, which means those requiring the minimum adjustment to fluxes from prior to posterior.

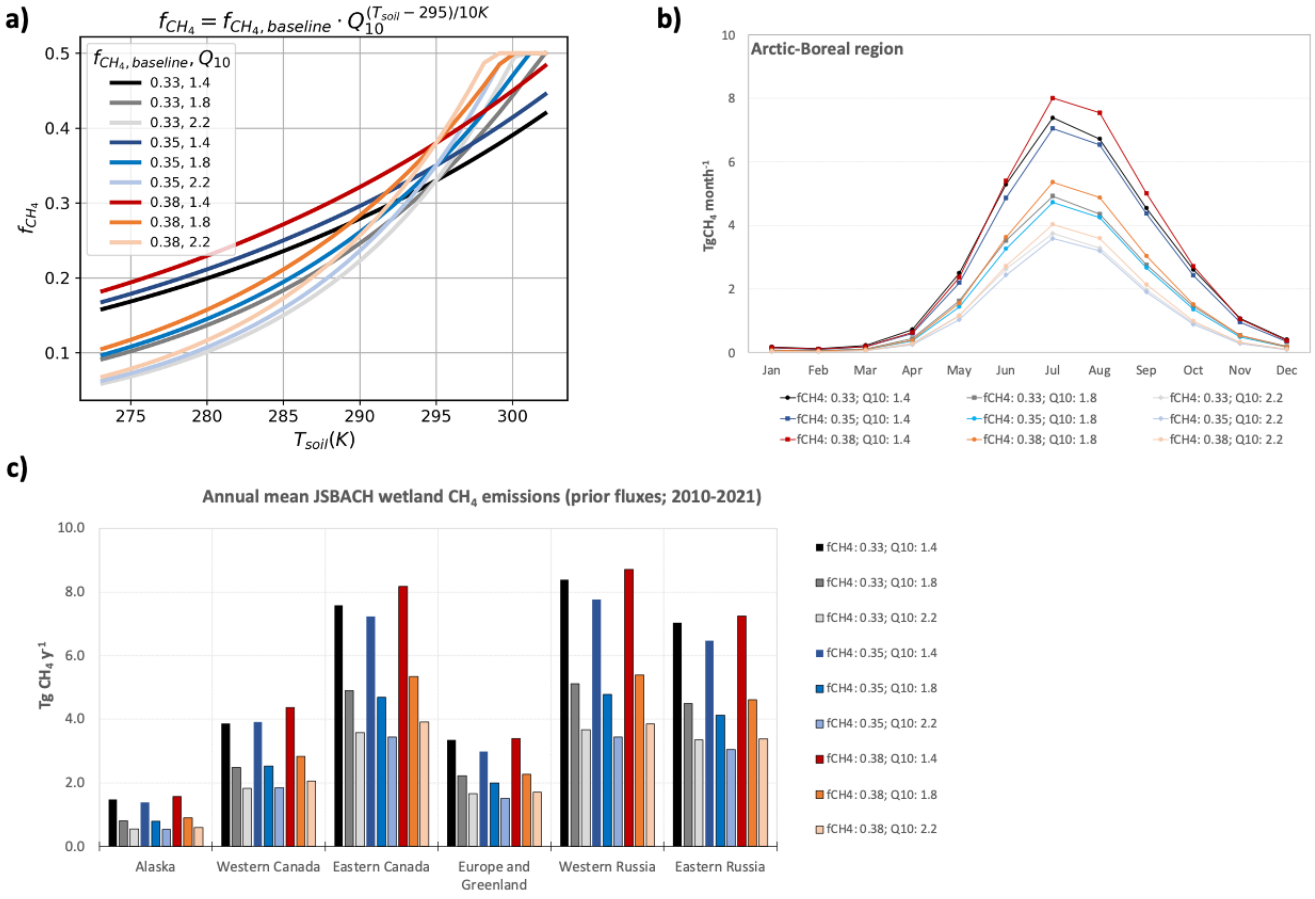

Figure 2. a) Sensitivity of f_{CH_4} production fraction to the chosen range of input parameters for this study. The y-axis represents the fraction of anaerobic carbon mineralization allocated to CH_4 production, calculated using the equation displayed at the top of the panel and in Equation 1. In the legend, the first number denotes the f_{CH_4} baseline fraction and the second number denotes the CH_4 production Q_{10} value. b) Mean seasonal cycle of Arctic-Boreal wetland CH_4 emissions for each experiment used in the inversion as the wetland prior flux. c) Annual mean wetland fluxes from each experiment estimated by JSBACH model.

3.2 Evaluation of JSBACH CH_4 Fluxes Using Inverse Modeling

Our nine inverse model estimates produce an annual mean total emission (i.e. including natural and anthropogenic sources) for the Arctic-Boreal region ranging from 44.2 to 47.1 $TgCH_4\ y^{-1}$, with wetland emissions being the main CH_4 source

to the atmosphere. Depending on the parameter set in the prior flux setup by JSBACH, the annual mean wetland emission ranges from 20.9 to 25.0 $TgCH_4\ y^{-1}$ (47-54% of total emissions). The largest posterior wetland CH_4 emissions were estimated for western Russia (range of 6.9-8.4 $TgCH_4\ y^{-1}$, depending on the parameter set), followed by eastern Russia (range of 6.0-7.5 $TgCH_4\ y^{-1}$), eastern Canada (range of 4.3-4.9 $TgCH_4\ y^{-1}$), western Canada (range of 1.7-1.8 $TgCH_4\ y^{-1}$), Alaska (range of 1.0-2.0 $TgCH_4\ y^{-1}$) and Europe including Greenland (range of 0.7-0.8 $TgCH_4\ y^{-1}$)

At the pan-Arctic scale, posterior wetland fluxes are higher than prior fluxes in the experiments using CH_4 production Q_{10} values of 1.8 (8-22% higher than prior) and 2.2 (37-54% higher), see Table 1 and Fig. 3a. This suggests that these prior estimates underestimate CH_4 emissions in the Arctic-Boreal region relative to the observation-constrained posterior fluxes. However, prior fluxes estimated using a Q_{10} value of 1.4 are higher than posterior fluxes (16-25% higher than posterior), indicating overestimation of CH_4 emissions in this case. When comparing the model adjustment for the three experiments (varying only the Q_{10} parameters), the prior flux using Q_{10} values of 1.8 produces the best agreement between prior and posterior flux budgets, meaning that a minimum adjustment in the inverse model optimization is required when considering annual mean emissions in the entire Arctic-Boreal region. Additionally, when comparing the different baseline f_{CH_4} fractions (using the Q_{10} value with the best fit: 1.8), the minimum adjustment in the inverse model optimization is required for the prior flux with the largest baseline f_{CH_4} fraction (0.38), with posterior flux being 8% (2.0 $TgCH_4\ y^{-1}$) higher than the prior.

Our posterior estimates of CH_4 emissions from wetlands are similar to previous Arctic-Boreal estimates. Using a process-oriented ecosystem model, Christensen et al. (1996) estimated a total CH_4 emissions from northern wetlands and tundra (> 50°N) to be 20 ± 13 $TgCH_4\ y^{-1}$. Yuan et al. (2024) reported a mean annual emission of 20.3 ± 0.9 $TgCH_4\ y^{-1}$ from Boreal-Arctic wetland based on upscaled flux observations for the period 2002-2021. The Global Carbon Project estimated a mean annual wetland (including inland freshwaters) CH_4 emission for regions north of 60°N at 24 (9-53) $TgCH_4\ y^{-1}$, while top-down approaches resulted in a lower estimate of 9 (7-17) $TgCH_4\ y^{-1}$ for the same region (Saunois et al., 2025). Recently, Ying et al. (2025)estimated an annual mean CH_4 emissions from vegetated wetlands north of 45°N during 2016-2022 at 22.8 ± 2.4 $TgCH_4\ y^{-1}$, ranging from 15.7 ± 1.8 $TgCH_4\ y^{-1}$ to 51.6 ± 2.2 $TgCH_4\ y^{-1}$, depending on the wetland dataset used in the machine-learning-based upscaling approach. Although our posterior estimates are within the range of previous Arctic-Boreal estimates, direct comparisons are difficult because of differences in the study period, methodological approach, and inconsistent or unclear definitions of the spatial domain.

3.3 Seasonal variability in optimum CH_4 production Q_{10} settings

Before analyzing regional differences in optimum CH_4 production Q_{10} settings, we first focused on a clear seasonal pattern in the adjustments between prior and posterior CH_4 emissions, which showed a peak of changes occurring during summer. We therefore assessed whether the Q_{10} value resulting in the minimum adjustment remained constant throughout the year or varied by season. At a pan-Arctic scale, seasonal variations were evident: estimates using CH_4 production Q_{10} equaling 1.8 aligned better with atmospheric observations in spring and fall but substantially underestimated summer emissions (Fig. 3b). In contrast, estimates using a Q_{10} of 1.4 best aligned with the atmospheric observation during summer, reducing the

discrepancy between top-down and bottom-up estimates during the growing season, but strongly overestimating emissions in spring and fall (Fig. 3b). This pattern is primarily driven by wetlands in Russia. Bergman et al. (2000) found temporal variation in Q_{10} at peatland sites, suggesting that factors such as the availability of easily degradable compounds (e.g., root exudates) and the activity of anaerobic microbial biomass influence CH_4 production rates alongside temperature.

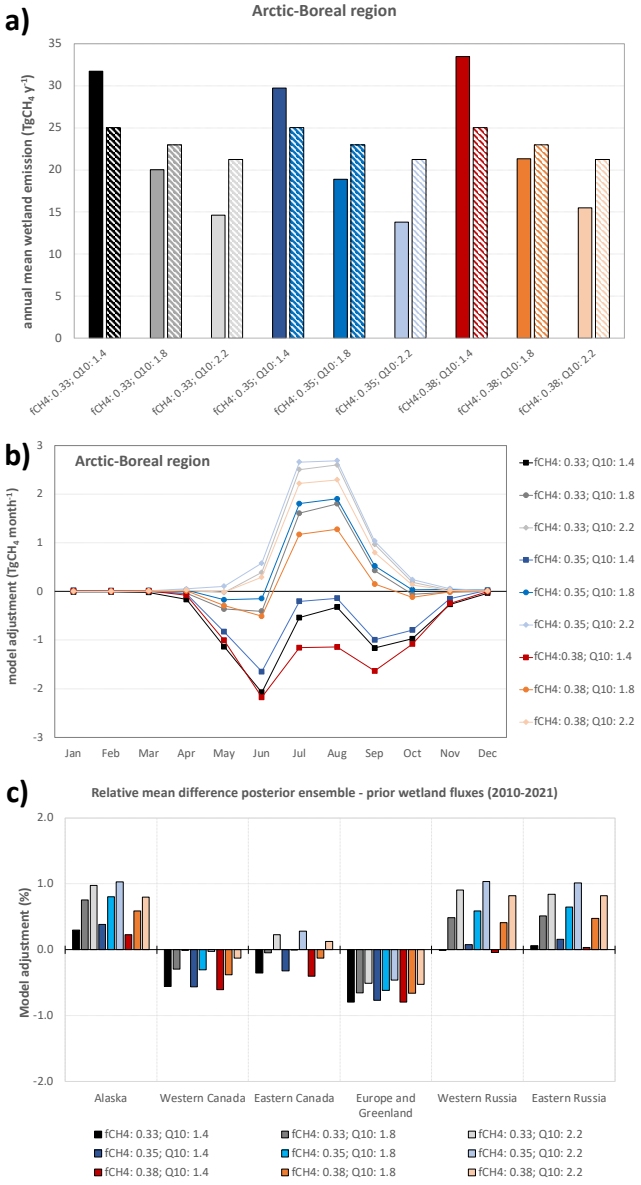

Figure 3. a) Annual mean CH_4 emissions (prior: full color bars; posterior: dashed color bars) for the entire Arctic-Boreal region using all nine inversion scenarios with the different values of Q_{10} parameter and baseline f_{CH_4} fraction in JSBACH wetland emissions. b) adjustment of prior fluxes at monthly timesteps for the same model configurations as used in (a). c) relative annual mean model adjustment as percentage of prior (posterior ensemble minus prior flux) for each one of the sub-regions. Positive values indicate regions where prior estimates underestimated emissions compared with posterior estimates, while negative values represent areas where prior emissions overestimate CH_4 emissions compared with the posterior estimates.

3.4. Spatial patterns of best-fit model results based on posterior fluxes

CH_4 emissions exhibited spatial variability, and model adjustments were not uniform across the domain. This suggests that the optimal parameterization varies by region and seasons (as discussed in Section 3.3). In some areas, Q_{10} values of 1.4 or 2.2 resulted in minimal adjustments (Fig. 3c), outperforming the model using a Q_{10} equaling 1.8 that was shown to work best as an average setting across the entire domain. To better evaluate this variability and explore ways to reduce uncertainty in specific regions, we assessed the best parameterization fit with observations at the per grid-cell level (Fig. 4).

In our first analysis, we evaluated the spatial best fit model by keeping the baseline constant at a value of 0.35 and varying the CH_4 production Q_{10} values (Fig. 4a). This spatial analysis showed that, in general, in regions with large wetland areas and high annual CH_4 emissions (for example the Western Siberian Lowlands, Supplementary Fig. 1 and 2) a Q_{10} value of 1.4 resulted in the smallest model adjustment. As an increase in the Q_{10} parameter decreases CH_4 production for temperatures below 295 K, a higher Q_{10} value in these regions results in an underestimation of emissions. In contrast, regions such as Europe and northern Canada showed, in general, minimum model adjustments with a Q_{10} value of 2.2, suggesting that lower Q_{10} value would overestimate wetland CH_4 emissions in these regions. Interestingly, we observed adjustments with different signs in eastern Canada depending on the parameterization. For example, positive adjustments were associated with Q_{10} value of 2.2, as the prior emissions were underestimated compared with the estimated flux inferred from atmospheric observations. Additionally, we analyzed the effect of varying baseline flux values while keeping Q_{10} constant as 1.8, which showed that in high-emission areas, for example the Western Siberian Lowlands (Supplementary Fig. 1 and 2), in general a larger baseline flux value led to the smallest model adjustments (Fig. 4b). When considering the model adjustment for all sensitivity tests (varying both CH_4 production Q_{10} and baseline f_{CH_4} fraction) as shown in Fig. 4c, we also found a consistent pattern that confirmed the above findings varying only single parameters: the combination of higher baseline fluxes and lower Q_{10} value (Q_{10} = 1.4) best captured CH_4 dynamics in CH_4 hotspots, as the Western Siberia Lowlands.

The wide range of reported incubation-based Q_{10} values for CH_4 production in Arctic and northern wetlands depending on the site, substrate, and season, shows that the temperature sensitivity of CH_4 production varies considerably across environments (Bergman et al., 2000; Roy Chowdhury et al., 2015; Treat et al., 2015). This variability, which could be driven by factors such as vegetation type, organic matter quality, and microbial activity, emphasizes the necessity of models to account for spatial differences in process rates. For example, one synthesis study reported a mean Q_{10} value of 1.18 for CH_4 production under Arctic soil conditions (Roy Chowdhury et al., 2015; Treat et al., 2015). Roy Chowdhury et al. (2015) used anoxic laboratory incubations of active layer and permafrost samples from the Barrow Environmental Observatory in Alaska and reported a range of Q_{10} values from 1.8 to 22. Lupascu et al. (2012) reported that Q_{10} values describing the CH_4 production response of peat to a 10 °C temperature change ranged from 1.9 to 3.5 in sedge sites and from 2.4 to 5.8 in *Sphagnum* mire sites, and suggested that using spatially variable CH_4 production Q_{10} values could improve the accuracy of CH_4 flux modeling in northern wetlands. Furthermore, Bergman et al. (2000) found that the seasonal average Q_{10} values ranged from approximately 4.6 to 9.2 depending on the plant community of the various peat types. Here, our intent is not to directly compare our results with reported incubation-based values, since our adjustments in the CH_4 production Q_{10} refer to the Q_{10} of the

CH_4:CO_2 production ratio, as represented in the model, and could not directly be comparable with CH_4 production Q_{10} from the literature review. In JSBACH, the Q_{10} applied to CH_4 production controls the fraction of CH_4 generated, but the surface emission ratio may still be lower due to oxidation and transport pathways. Together, these examples highlight that CH_4 production is strongly temperature dependent, and that the degree of this dependency can differ across regions and time periods. However, most current models cannot fully capture the influence of these factors due to structural limitations or a lack of detailed input data that is both spatially and temporally resolved. Consequently, these environmental drivers are often oversimplified or overlooked. Adjusting the CH_4 production Q_{10} values, as we do here, offers a useful initial approach, but it should not be seen as a long-term solution. Ideally, future model and data developments will enable CH_4 production Q_{10} values to adjust dynamically in response to underlying biophysical conditions, such as shifts in vegetation or organic matter characteristics. This will allow models to operate with a more generalizable formulation that still captures observed heterogeneity. Recent studies have demonstrated the potential of methane data assimilation techniques to optimize process-model parameters using observational constraints (Bernard et al., 2025; Monteil et al., 2025); however, regional and seasonal optimization remains largely unexplored. While our model experiments identified a single CH_4 production Q_{10} value that best agrees with observations at the pan-Arctic scale, they also showed that CH_4 emissions and model adjustments vary regionally. Some areas showed a substantial response to different Q_{10} values, which further demonstrates that an approach using a single parameter value is not sufficient. This highlights the need for future data assimilation frameworks that allow for regional, and potentially seasonal, parameter optimization.

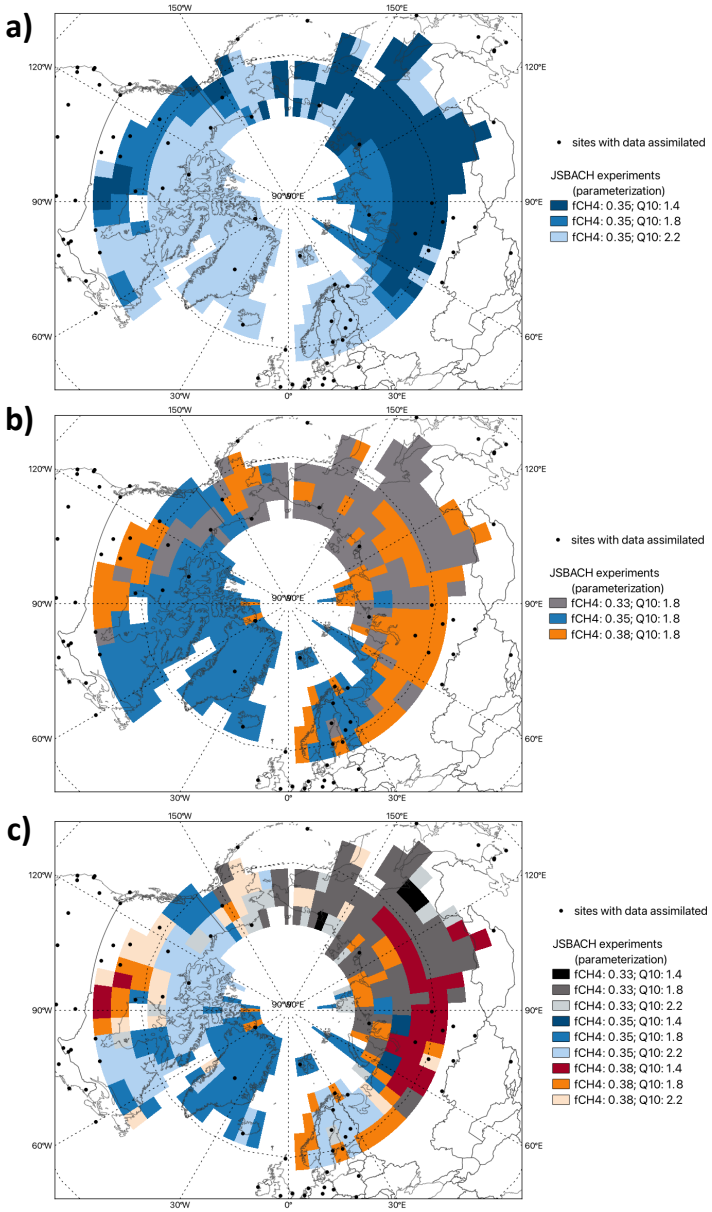

Figure 4. Map of the prior flux setting leading to minimum model adjustment (posterior ensemble minus prior fluxes) for the annual mean fluxes at each grid-cell for the Arctic-Boreal region varying the (a) CH_4 production Q_{10} parameter only, (b) baseline f_{CH_4} fraction only and (c) both Q_{10} parameter and baseline f_{CH_4} fraction. As mentioned in Section 3.2, the configuration with Q_{10} = 1.8 and f_{CH_4} = 0.38 provides the best fit at the pan-Arctic scale. However, regional results show that this configuration does not minimize flux adjustments everywhere.

3.5. Limitations of Top-Down CH_4 estimates

Our analysis shows that atmospheric inverse modeling is a useful tool for evaluating and guiding process-model parameterizations when estimating wetland CH_4 emissions. However, it is important to note the limitations of the top-down

approach, especially its relatively coarse spatial resolution. Global inversions usually operate at spatial scales larger than the process models, limiting their ability to resolve fine-scale heterogeneity, local emission hotspots, and small-scale processes. Consequently, grid-cell-level emission estimates represent aggregated signals and cannot fully capture localized variability.

Additionally, top-down estimates rely heavily on the spatial and temporal distribution of atmospheric observations assimilated into the model. Regions with sparce coverage, such as central and eastern Russia, can limit the ability to accurately identify emission sources and increase dependence on prior estimates. Furthermore, most surface observation sites at high latitudes only started providing measurements in the early 2010s. This limits the ability to assess multi-decadal changes in CH_4 emissions (Vogt et al., 2025).

At the grid-cell scale, assimilating only atmospheric CH_4 observations reflect the combined influence of all sources and sinks, making it difficult to distinguish overlapping source sectors. However, differences in the spatial patterns and seasonality of emissions can be constrained by atmospheric CH_4 observations in inversions that solve for different source categories (Saunois et al., 2025). Furthermore, errors in atmospheric transport model can propagate into emission estimates (Houweling et al., 2017; Locatelli et al., 2013; Schuh et al., 2019). Despite these limitations, our approach demonstrated a strong potential to help reduce the discrepancy between bottom-up and top-down estimates, therefore improving the accuracy of wetland CH_4 emission estimates.

4. Conclusions

Overall, our parameter sensitivity tests of bottom-up wetland emissions indicate that CH_4 production Q_{10} has a stronger effect on emission variability than the baseline f_{CH_4} fraction. Our bottom-up estimates showed that increasing CH_4 production Q_{10} from 1.4 to 2.2 decreased the annual mean wetland CH_4 emission in the Arctic–Boreal region by half. In addition, our analysis shows that a single Q_{10} value cannot capture the complexity of CH_4 emission dynamics across the Arctic-Boreal region. CH_4 production Q_{10} values of 1.8 and 2.2 underestimate hotspot emissions, mainly during summer. In contrast, a Q_{10} value of 1.4 overestimates emissions in regions with lower annual mean wetland emissions, such as e.g., Europe and northern Canada. Furthermore, a baseline f_{CH_4} fraction value of 0.38 led to the smallest model adjustments in CH_4 hotspots. These findings emphasize the importance of selecting appropriate parameterizations to accurately represent wetland emissions, especially in regions with substantial CH_4 release. Future models should incorporate dynamic, data-driven adjustments to reflect underlying environmental controls more accurately. If a varying CH_4 production Q_{10} value approach is not feasible for this region due to computational cost or model setup constraints, using a Q_{10} value of 1.8 provides the more similar CH_4 emission estimates compared to the atmospheric data across the entire Arctic-Boreal region.

Our results demonstrate that, despite the inherent limitations of top-down approaches when it comes to resolving fine scale heterogeneity, combining atmospheric inversions and process-models provides an important tool for reconciling discrepancies between bottom-up and top-down estimates, thereby improving constraints on large-scale wetland methane emissions.

Guidance by atmospheric inversion could therefore be instrumental to ensure the regional representativeness, and where applicable temporal variability, of process model parameter settings.

5. Authors contributions

LSB, MG, GG, VB designed the methodology. LSB wrote the first version of the manuscript and performed analysis and CH_4 inversions. GG performed and provided the JSBACH simulations. CR provided guidance and technical support for the inverse modelling. CB provided additional input on the discussion of results. All authors contributed with analysis and text. MG supervised and acquired funding.

6. Data and code availability

The prior and posterior mean Arctic-Boreal CH_4 fluxes on the CarboScope model horizontal resolution will be available in a data repository if the paper is accepted for publication. Observations from the NOAA GML network can be downloaded from the dedicated Observation Package (ObsPack) web server at http://doi.org/10.25925/20231001. The dataset "European atmospheric CO_2, CH_4 and N_2O Mole Fraction data product – 2024" analyzed during the current study was downloaded from the ICOS Carbon portal, DOI: https://doi.org/10.18160/KDMT-V6CG. The observations from the WDCGG dataset are available at https://doi.org/10.50849/WDCGG_CH4_ALL_2023. ATTO tower data can be request at https://www.attodata.org/. Observations from the Japan-Russia Siberian Tall Tower Inland Observation Network (JR-STATION (Sasakawa et al., 2010) can be downloaded from https://doi.org/10.17595/20231117.001, https://doi.org/10.17595/20231117.002, https://doi.org/10.17595/20231117.004, https://doi.org/10.17595/20231117.005, https://doi.org/10.17595/20231117.006, https://doi.org/10.17595/20231117.007, https://doi.org/10.17595/20231117.008. CH_4 observations from the western Taimyr Peninsula (Siberia) can be downloaded from http://doi.org/10.17632/gcts3dddrh.1.

7. Competing interests

The authors declare that they have no conflict of interest.

8. Acknowledgements

The authors were funded by the European Research Council (ERC synergy project Q-Arctic, grant agreement no. 951288), the German Federal Ministry of Research, Technology and Space (MOMENT project, support code 03F0931G), and the AMPAC-net initiative (European Space Agency, grant no. 4000137912/22/I-DT). The authors would also like to thank Dr. Santiago Botía at MPI-BGC/BSI for his valuable comments and suggestions, which helped us to improve this manuscript. The authors

would like to acknowledge the contributions of Tonatiuh Nunez Ramirez, who designed the CH_4 chemistry model for CarboScope inversion system used in this work.

We would like to thank all Principal Investigators and supporting staff for setting up and maintaining observation sites around the world, particularly in the Arctic, and for making the data available through different databases, including NOAA Obspack, ICOS RI, WDCGG and JR-STATION. The ICOS activities at Ricerca sul Sistema Energetico (PRS) station are financed by the Research Fund for the Italian Electrical System under the Three-Year Research Plan 2025-2027 (MASE, Decree n.388 of November 6th, 2024), in compliance with the Decree of April 12th, 2024. Although not fundamental to our study, we use ATTO methane data from 2012 to 2019 and for this we want to acknowledge Jost Lavric and the ATTO consortium for making the data available. This work is based on use of Large Research Infrastructure CzeCOS supported by the Ministry of Education, Youth and Sports of CR within the CzeCOS program, grant number LM2023048.

Parts of the text was language-edited for grammatical correctness using DeepL. The authors have reviewed and verified the content as needed and take full responsibility for it.

9. References

Bergman, I., Klarqvist, M., and Nilsson, M.: Seasonal variation in rates of methane production from peat of various botanical origins: effects of temperature and substrate quality, FEMS Microbiol. Ecol., 33, 181–189, https://doi.org/10.1111/j.1574-6941.2000.tb00740.x, 2000.

Bernard, J., Salmon, E., Saunois, M., Peng, S., Serrano-Ortiz, P., Berchet, A., Gnanamoorthy, P., Jansen, J., and Ciais, P.: Satellite-based modeling of wetland methane emissions on a global scale (SatWetCH4 1.0), Geosci. Model Dev., 18, 863–883, https://doi.org/10.5194/gmd-18-863-2025, 2025.

BEVEN, K. J. and KIRKBY, M. J.: A physically based, variable contributing area model of basin hydrology / Un modèle à base physique de zone d'appel variable de l'hydrologie du bassin versant, Hydrological Sciences Bulletin, 24, 43–69, https://doi.org/10.1080/02626667909491834, 1979.

Chinta, S., Gao, X., and Zhu, Q.: Machine Learning Driven Sensitivity Analysis of E3SM Land Model Parameters for Wetland Methane Emissions, J. Adv. Model. Earth Syst., 16, https://doi.org/10.1029/2023MS004115, 2024.

Christensen, T. R., Prentice, I. C., Kaplan, J., Haxeltine, A., and Sitch, S.: Methane flux from northern wetlands and tundra, Tellus B: Chemical and Physical Meteorology, 48, 652, https://doi.org/10.3402/tellusb.v48i5.15938, 1996.

Conrad, R.: Contribution of hydrogen to methane production and control of hydrogen concentrations in methanogenic soils and sediments, FEMS Microbiol. Ecol., 28, 193–202, https://doi.org/10.1111/j.1574-6941.1999.tb00575.x, 1999.

Crippa, M., Guizzardi, D., Pagani, F., Banja, M., Muntean, M., Schaaf E., Becker, W., Monforti-Ferrario, F., Quadrelli, R., Risquez Martin, A., Taghavi-Moharamli, P., Köykkä, J., Grassi, G., Rossi, S., Brandao De Melo, J., Oom, D., Branco, A., San-Miguel, J., and Vignati, E.: GHG emissions of all world countries, Luxembourg, https://doi.org/https://data.europa.eu/doi/10.2760/953322, 2023.

Ekici, A., Beer, C., Hagemann, S., Boike, J., Langer, M., and Hauck, C.: Simulating high-latitude permafrost regions by the JSBACH terrestrial ecosystem model, Geosci. Model Dev., 7, 631–647, https://doi.org/10.5194/gmd-7-631-2014, 2014.

Etiope, G., Ciotoli, G., Schwietzke, S., and Schoell, M.: Gridded maps of geological methane emissions and their isotopic signature, Earth Syst. Sci. Data, 11, 1–22, https://doi.org/10.5194/essd-11-1-2019, 2019.

Goll, D. S., Brovkin, V., Liski, J., Raddatz, T., Thum, T., and Todd-Brown, K. E. O.: Strong dependence of CO_2 emissions from anthropogenic land cover change on initial land cover and soil carbon parametrization, Global Biogeochem. Cycles, 29, 1511–1523, https://doi.org/10.1002/2014GB004988, 2015.

Guimberteau, M., Zhu, D., Maignan, F., Huang, Y., Yue, C., Dantec-Nédélec, S., Ottlé, C., Jornet-Puig, A., Bastos, A., Laurent, P., Goll, D., Bowring, S., Chang, J., Guenet, B., Tifafi, M., Peng, S., Krinner, G., Ducharne, A., Wang, F., Wang, T., Wang, X., Wang, Y., Yin, Z., Lauerwald, R., Joetzjer, E., Qiu, C., Kim, H., and Ciais, P.: ORCHIDEE-MICT (v8.4.1), a land surface model for the high latitudes: model description and validation, Geosci. Model Dev., 11, 121–163, https://doi.org/10.5194/gmd-11-121-2018, 2018.

Hagemann, S. and Stacke, T.: Impact of the soil hydrology scheme on simulated soil moisture memory, Clim. Dyn., 44, 1731–1750, https://doi.org/10.1007/s00382-014-2221-6, 2015.

Harris, I. C.: CRUJRA: Collection of CRUJRA forcing datasets of gridded land surface blend of Climatic Research Unit (CRU) and Japanese reanalysis (JRA) data.Centre for Environmental Data Analysis, University of East Anglia Climatic Research Unit., 2019.

Heimann, M. and Körner, S.: The global atmospheric tracer model TM3: model description and user's manual release 3.8a, Jena, 2003.

Hossaini, R., Chipperfield, M. P., Saiz-Lopez, A., Fernandez, R., Monks, S., Feng, W., Brauer, P., and Glasow, R. von: A global model of tropospheric chlorine chemistry: Organic versus inorganic sources and impact on methane oxidation, Journal of Geophysical Research: Atmospheres, 121, 14,271-14,297, https://doi.org/10.1002/2016JD025756, 2016.

Houweling, S., Bergamaschi, P., Chevallier, F., Heimann, M., Kaminski, T., Krol, M., Michalak, A. M., and Patra, P.: Global inverse modeling of CH_4 sources and sinks: an overview of methods, Atmos. Chem. Phys., 17, 235–256, https://doi.org/10.5194/acp-17-235-2017, 2017.

Hugelius, G., Ramage, J., Burke, E., Chatterjee, A., Smallman, T. L., Aalto, T., Bastos, A., Biasi, C., Canadell, J. G., Chandra, N., Chevallier, F., Ciais, P., Chang, J., Feng, L., Jones, M. W., Kleinen, T., Kuhn, M., Lauerwald, R., Liu, J., López-Blanco, E., Luijkx, I. T., Marushchak, M. E., Natali, S. M., Niwa, Y., Olefeldt, D., Palmer, P. I., Patra, P. K., Peters, W., Potter, S., Poulter, B., Rogers, B. M., Riley, W. J., Saunois, M., Schuur, E. A. G., Thompson, R. L., Treat, C., Tsuruta, A., Turetsky, M. R., Virkkala, A. -M., Voigt, C., Watts, J., Zhu, Q., and Zheng, B.: Permafrost Region Greenhouse Gas Budgets Suggest a Weak CO_2 Sink and CH_4 and N_2O Sources, But Magnitudes Differ Between Top-Down and Bottom-Up Methods, Global Biogeochem. Cycles, 38, https://doi.org/10.1029/2023GB007969, 2024.

ICOS RI, Bergamaschi, P., Colomb, A., De Mazière, M., Emmenegger, L., Kubistin, D., Lehner, I., Lehtinen, K., Lund Myhre, C., Marek, M., O'Doherty, S., Platt, S. M., Plaß-Dülmer, C., Ramonet, M., Apadula, F., Arnold, S., Blanc, P.-E., Brunner, D.,

Chen, H., Chmura, L., Conil, S., Couret, C., Cristofanelli, P., Delmotte, M., Forster, G., Frumau, A., Gheusi, F., Hammer, S., Haszpra, L., Hatakka, J., Heliasz, M., Henne, S., Hoheisel, A., Kneuer, T., Laurila, T., Leskinen, A., Leuenberger, M., Levin, I., Lindauer, M., Lunder, C., Mammarella, I., Manca, G., Manning, A., Martin, D., Meinhardt, F., Mölder, M., Müller-Williams, J., Necki, J., Ottosson-Löfvenius, M., Philippon, C., Piacentino, S., Pitt, J., Rivas-Soriano, P., Scheeren, B., Schumacher, M., Sha, M. K., Smith, P., Spain, G., Steinbacher, M., Sørensen, L. L., Vermeulen, A., Vítková, G., Xueref-Remy, I., di Sarra, A., Conen, F., Kazan, V., Roulet, Y.-A., Biermann, T., Heltai, D., D.Hensen, A., Hermansen, O., Komínková, K., Laurent, O., Levula, J., Lopez, M., Marklund, P., Pichon, J.-M., Schmidt, M., Stanley, K., and Trisolino, P.: European Obspack compilation of atmospheric methane data from ICOS and non-ICOS European stations for the period 1984-2024; obspack_ch4_466_GVeu_2024-02-01, https://doi.org/https://doi.org/10.18160/KDMT-V6CG, 2024.

Jöckel, P., Tost, H., Pozzer, A., Brühl, C., Buchholz, J., Ganzeveld, L., Hoor, P., Kerkweg, A., Lawrence, M. G., Sander, R., Steil, B., Stiller, G., Tanarhte, M., Taraborrelli, D., van Aardenne, J., and Lelieveld, J.: The atmospheric chemistry general circulation model ECHAM5/MESSy1: consistent simulation of ozone from the surface to the mesosphere, Atmos. Chem. Phys., 6, 5067–5104, https://doi.org/10.5194/acp-6-5067-2006, 2006.

Kalnay, E., Kanamitsu, M., Kistler, R., Collins, W., Deaven, D., Gandin, L., Iredell, M., Saha, S., White, G., Woollen, J., Zhu, Y., Leetmaa, A., Reynolds, R., Chelliah, M., Ebisuzaki, W., Higgins, W., Janowiak, J., Mo, K. C., Ropelewski, C., Wang, J., Jenne, R., and Joseph, D.: The NCEP/NCAR 40-Year Reanalysis Project, Bull. Am. Meteorol. Soc., 77, 437–471, https://doi.org/10.1175/1520-0477(1996)077<0437:TNYRP>2.0.CO;2, 1996.

Kim, H.-S., Maksyutov, S., Glagolev, M. V, Machida, T., Patra, P. K., Sudo, K., and Inoue, G.: Evaluation of methane emissions from West Siberian wetlands based on inverse modeling, Environmental Research Letters, 6, 035201, https://doi.org/10.1088/1748-9326/6/3/035201, 2011.

Kleinen, T., Mikolajewicz, U., and Brovkin, V.: Terrestrial methane emissions from the Last Glacial Maximum to the preindustrial period, Climate of the Past, 16, 575–595, https://doi.org/10.5194/cp-16-575-2020, 2020.

Knoblauch, C., Beer, C., Liebner, S., Grigoriev, M. N., and Pfeiffer, E.-M.: Methane production as key to the greenhouse gas budget of thawing permafrost, Nat. Clim. Chang., 8, 309–312, https://doi.org/10.1038/s41558-018-0095-z, 2018.

Locatelli, R., Bousquet, P., Chevallier, F., Fortems-Cheney, A., Szopa, S., Saunois, M., Agusti-Panareda, A., Bergmann, D., Bian, H., Cameron-Smith, P., Chipperfield, M. P., Gloor, E., Houweling, S., Kawa, S. R., Krol, M., Patra, P. K., Prinn, R. G., Rigby, M., Saito, R., and Wilson, C.: Impact of transport model errors on the global and regional methane emissions estimated by inverse modelling, Atmos. Chem. Phys., 13, 9917–9937, https://doi.org/10.5194/acp-13-9917-2013, 2013.

Lupascu, M., Wadham, J. L., Hornibrook, E. R. C., and Pancost, R. D.: Temperature Sensitivity of Methane Production in the Permafrost Active Layer at Stordalen, Sweden: A Comparison with Non-permafrost Northern Wetlands, Arct. Antarct. Alp. Res., 44, 469–482, https://doi.org/10.1657/1938-4246-44.4.469, 2012.

Mauritsen, T., Bader, J., Becker, T., Behrens, J., Bittner, M., Brokopf, R., Brovkin, V., Claussen, M., Crueger, T., Esch, M., Fast, I., Fiedler, S., Fläschner, D., Gayler, V., Giorgetta, M., Goll, D. S., Haak, H., Hagemann, S., Hedemann, C., Hohenegger, C., Ilyina, T., Jahns, T., Jimenéz-de-la-Cuesta, D., Jungclaus, J., Kleinen, T., Kloster, S., Kracher, D., Kinne, S., Kleberg, D.,

Lasslop, G., Kornblueh, L., Marotzke, J., Matei, D., Meraner, K., Mikolajewicz, U., Modali, K., Möbis, B., Müller, W. A., Nabel, J. E. M. S., Nam, C. C. W., Notz, D., Nyawira, S., Paulsen, H., Peters, K., Pincus, R., Pohlmann, H., Pongratz, J., Popp, M., Raddatz, T. J., Rast, S., Redler, R., Reick, C. H., Rohrschneider, T., Schemann, V., Schmidt, H., Schnur, R., Schulzweida, U., Six, K. D., Stein, L., Stemmler, I., Stevens, B., von Storch, J., Tian, F., Voigt, A., Vrese, P., Wieners, K., Wilkenskjeld, S., Winkler, A., and Roeckner, E.: Developments in the MPI-M Earth System Model version 1.2 (MPI-ESM1.2) and Its Response to Increasing CO_2, J. Adv. Model. Earth Syst., 11, 998–1038, https://doi.org/10.1029/2018MS001400, 2019.

Miller, S. M., Commane, R., Melton, J. R., Andrews, A. E., Benmergui, J., Dlugokencky, E. J., Janssens-Maenhout, G., Michalak, A. M., Sweeney, C., and Worthy, D. E. J.: Evaluation of wetland methane emissions across North America using atmospheric data and inverse modeling, Biogeosciences, 13, 1329–1339, https://doi.org/10.5194/bg-13-1329-2016, 2016.

Monteil, G., Theanutti Kallingal, J., and Scholze, M.: CH_4 emissions from Northern Europe wetlands: compared data assimilation approaches, Atmos. Chem. Phys., 25, 14251–14277, https://doi.org/10.5194/acp-25-14251-2025, 2025.

Moser, M., Kaiser, L., Brovkin, V., and Beer, C.: Reviews and syntheses: The role of process-based modeling of the CO_2 : CH_4 production ratio in predicting future terrestrial Arctic methane emissions, Biogeosciences, 23, 605–621, https://doi.org/10.5194/bg-23-605-2026, 2026.

Olefeldt, D., Hovemyr, M., Kuhn, M. A., Bastviken, D., Bohn, T. J., Connolly, J., Crill, P., Euskirchen, E. S., Finkelstein, S. A., Genet, H., Grosse, G., Harris, L. I., Heffernan, L., Helbig, M., Hugelius, G., Hutchins, R., Juutinen, S., Lara, M. J., Malhotra, A., Manies, K., McGuire, A. D., Natali, S. M., O'Donnell, J. A., Parmentier, F.-J. W., Räsänen, A., Schädel, C., Sonnentag, O., Strack, M., Tank, S. E., Treat, C., Varner, R. K., Virtanen, T., Warren, R. K., and Watts, J. D.: The Boreal–Arctic Wetland and Lake Dataset (BAWLD), Earth Syst. Sci. Data, 13, 5127–5149, https://doi.org/10.5194/essd-13-5127-2021, 2021.

Panov, A., Prokushkin, A., Kübler, K. R., Korets, M., Urban, A., Bondar, M., and Heimann, M.: Continuous CO2 and CH4 Observations in the Coastal Arctic Atmosphere of the Western Taimyr Peninsula, Siberia: The First Results from a New Measurement Station in Dikson, Atmosphere (Basel)., 12, 876, https://doi.org/10.3390/atmos12070876, 2021.

Poulter, B., Bousquet, P., Canadell, J. G., Ciais, P., Peregon, A., Saunois, M., Arora, V. K., Beerling, D. J., Brovkin, V., Jones, C. D., Joos, F., Gedney, N., Ito, A., Kleinen, T., Koven, C. D., McDonald, K., Melton, J. R., Peng, C., Peng, S., Prigent, C., Schroeder, R., Riley, W. J., Saito, M., Spahni, R., Tian, H., Taylor, L., Viovy, N., Wilton, D., Wiltshire, A., Xu, X., Zhang, B., Zhang, Z., and Zhu, Q.: Global wetland contribution to 2000–2012 atmospheric methane growth rate dynamics, Environmental Research Letters, 12, 094013, https://doi.org/10.1088/1748-9326/aa8391, 2017.

Rantanen, M., Karpechko, A. Yu., Lipponen, A., Nordling, K., Hyvärinen, O., Ruosteenoja, K., Vihma, T., and Laaksonen, A.: The Arctic has warmed nearly four times faster than the globe since 1979, Commun. Earth Environ., 3, 168, https://doi.org/10.1038/s43247-022-00498-3, 2022.

Reick, C. H., Gayler, V., Goll, D., Hagemann, S., Heidkamp, M., Nabel, J. E. M. S., Raddatz, T., Roeckner, E., Schnur, R., and Wilkenskjeld, S.: JSBACH 3 - The land component of the MPI Earth System Model: documentation of version 3.2, 2021.

Ricciuto, D. M., Xu, X., Shi, X., Wang, Y., Song, X., Schadt, C. W., Griffiths, N. A., Mao, J., Warren, J. M., Thornton, P. E., Chanton, J., Keller, J. K., Bridgham, S. D., Gutknecht, J., Sebestyen, S. D., Finzi, A., Kolka, R., and Hanson, P. J.: An Integrative Model for Soil Biogeochemistry and Methane Processes: I. Model Structure and Sensitivity Analysis, J. Geophys. Res. Biogeosci., 126, https://doi.org/10.1029/2019JG005468, 2021.

Riley, W. J., Subin, Z. M., Lawrence, D. M., Swenson, S. C., Torn, M. S., Meng, L., Mahowald, N. M., and Hess, P.: Barriers to predicting changes in global terrestrial methane fluxes: analyses using CLM4Me, a methane biogeochemistry model integrated in CESM, Biogeosciences, 8, 1925–1953, https://doi.org/10.5194/bg-8-1925-2011, 2011.

Rödenbeck, C.: Estimating CO2 sources and sinks from atmo- spheric mixing ratio measurements using a global inversion of at- mospheric transport, Jena, 2005.

Roy Chowdhury, T., Herndon, E. M., Phelps, T. J., Elias, D. A., Gu, B., Liang, L., Wullschleger, S. D., and Graham, D. E.: Stoichiometry and temperature sensitivity of methanogenesis and <scp>CO</scp> 2 production from saturated polygonal tundra in Barrow, Alaska, Glob. Chang. Biol., 21, 722–737, https://doi.org/10.1111/gcb.12762, 2015.

Sasakawa, M., Shimoyama, K., Machida, T., Tsuda, N., Suto, H., Arshinov, M., Davydov, D., Fofonov, A., Krasnov, O., Saeki, T., Koyama, Y., and Maksyutov, S.: Continuous measurements of methane from a tower network over Siberia, Tellus B: Chemical and Physical Meteorology, 62, 403, https://doi.org/10.1111/j.1600-0889.2010.00494.x, 2010.

Sasakawa, M., Tsuda, N., Machida, T., Arshinov, M., Davydov, D., Fofonov, A., and Belan, B.: Revised methodology for CO 2 and CH 4 measurements at remote sites using a working standard-gas-saving system, Atmos. Meas. Tech., 18, 1717–1730, https://doi.org/10.5194/amt-18-1717-2025, 2025.

Saunois, M., Martinez, A., Poulter, B., Zhang, Z., Raymond, P. A., Regnier, P., Canadell, J. G., Jackson, R. B., Patra, P. K., Bousquet, P., Ciais, P., Dlugokencky, E. J., Lan, X., Allen, G. H., Bastviken, D., Beerling, D. J., Belikov, D. A., Blake, D. R., Castaldi, S., Crippa, M., Deemer, B. R., Dennison, F., Etiope, G., Gedney, N., Höglund-Isaksson, L., Holgerson, M. A., Hopcroft, P. O., Hugelius, G., Ito, A., Jain, A. K., Janardanan, R., Johnson, M. S., Kleinen, T., Krummel, P. B., Lauerwald, R., Li, T., Liu, X., McDonald, K. C., Melton, J. R., Mühle, J., Müller, J., Murguia-Flores, F., Niwa, Y., Noce, S., Pan, S., Parker, R. J., Peng, C., Ramonet, M., Riley, W. J., Rocher-Ros, G., Rosentreter, J. A., Sasakawa, M., Segers, A., Smith, S. J., Stanley, E. H., Thanwerdas, J., Tian, H., Tsuruta, A., Tubiello, F. N., Weber, T. S., van der Werf, G. R., Worthy, D. E. J., Xi, Y., Yoshida, Y., Zhang, W., Zheng, B., Zhu, Q., Zhu, Q., and Zhuang, Q.: Global Methane Budget 2000–2020, Earth Syst. Sci. Data, 17, 1873–1958, https://doi.org/10.5194/essd-17-1873-2025, 2025.

Schuh, A. E., Jacobson, A. R., Basu, S., Weir, B., Baker, D., Bowman, K., Chevallier, F., Crowell, S., Davis, K. J., Deng, F., Denning, S., Feng, L., Jones, D., Liu, J., and Palmer, P. I.: Quantifying the Impact of Atmospheric Transport Uncertainty on CO_2 Surface Flux Estimates, Global Biogeochem. Cycles, 33, 484–500, https://doi.org/10.1029/2018GB006086, 2019.

Schuldt, K. N., Mund, J., Aalto, T., Andrews, A., Apadula, F., Jgor Arduini, Arnold, S., Baier, B., Bäni, L., Bartyzel, J., Bergamaschi, P., Biermann, T., Biraud, S. C., Pierre-Eric Blanc, Boenisch, H., Brailsford, G., Brand, W. A., Brunner, D., Bui, T. P. V., and Miroslaw Zimnoch: Multi-laboratory compilation of atmospheric carbon dioxide data for the period 1983-2022;

609 obspack_ch4_1_GLOBALVIEWplus_v6.0_2023-12-01 [Data set]. NOAA Global Monitoring Laboratory.
610 http://doi.org/10.25925/20231001, 2023.
611 Sellar, A. A., Jones, C. G., Mulcahy, J. P., Tang, Y., Yool, A., Wiltshire, A., O'Connor, F. M., Stringer, M., Hill, R., Palmieri,
612 J., Woodward, S., de Mora, L., Kuhlbrodt, T., Rumbold, S. T., Kelley, D. I., Ellis, R., Johnson, C. E., Walton, J., Abraham, N.
613 L., Andrews, M. B., Andrews, T., Archibald, A. T., Berthou, S., Burke, E., Blockley, E., Carslaw, K., Dalvi, M., Edwards, J.,
614 Folberth, G. A., Gedney, N., Griffiths, P. T., Harper, A. B., Hendry, M. A., Hewitt, A. J., Johnson, B., Jones, A., Jones, C. D.,
615 Keeble, J., Liddicoat, S., Morgenstern, O., Parker, R. J., Predoi, V., Robertson, E., Siahaan, A., Smith, R. S., Swaminathan,
616 R., Woodhouse, M. T., Zeng, G., and Zerroukat, M.: UKESM1: Description and Evaluation of the U.K. Earth System Model,
617 J. Adv. Model. Earth Syst., 11, 4513–4558, https://doi.org/10.1029/2019MS001739, 2019.
618 Spahni, R., Wania, R., Neef, L., van Weele, M., Pison, I., Bousquet, P., Frankenberg, C., Foster, P. N., Joos, F., Prentice, I. C.,
619 and van Velthoven, P.: Constraining global methane emissions and uptake by ecosystems, Biogeosciences, 8, 1643–1665,
620 https://doi.org/10.5194/bg-8-1643-2011, 2011.
621 Spivakovsky, C. M., Logan, J. A., Montzka, S. A., Balkanski, Y. J., Foreman-Fowler, M., Jones, D. B. A., Horowitz, L. W.,
622 Fusco, A. C., Brenninkmeijer, C. A. M., Prather, M. J., Wofsy, S. C., and McElroy, M. B.: Three-dimensional climatological
623 distribution of tropospheric OH: Update and evaluation, Journal of Geophysical Research: Atmospheres, 105, 8931–8980,
624 https://doi.org/10.1029/1999JD901006, 2000.
625 Treat, C. C., Natali, S. M., Ernakovich, J., Iversen, C. M., Lupascu, M., McGuire, A. D., Norby, R. J., Roy Chowdhury, T.,
626 Richter, A., Šantrůčková, H., Schädel, C., Schuur, E. A. G., Sloan, V. L., Turetsky, M. R., and Waldrop, M. P.: A pan-Arctic
627 synthesis of CH_4 and CO_2 production from anoxic soil incubations, Glob. Chang. Biol., 21, 2787–2803,
628 https://doi.org/10.1111/gcb.12875, 2015.
629 Tuomi, M., Rasinmäki, J., Repo, A., Vanhala, P., and Liski, J.: Soil carbon model Yasso07 graphical user interface,
630 Environmental Modelling & Software, 26, 1358–1362, https://doi.org/10.1016/j.envsoft.2011.05.009, 2011.
631 Vogt, J., Pallandt, M. M. T. A., Basso, L. S., Bolek, A., Ivanova, K., Schlutow, M., Celis, G., Kuhn, M., Mauritz, M., Schuur,
632 E. A. G., Arndt, K., Virkkala, A.-M., Wargowsky, I., and Göckede, M.: ARGO: ARctic greenhouse Gas Observation metadata
633 version 1, Earth Syst. Sci. Data, 17, 2553–2573, https://doi.org/10.5194/essd-17-2553-2025, 2025.
634 Weber, T., Wiseman, N. A., and Kock, A.: Global ocean methane emissions dominated by shallow coastal waters, Nat.
635 Commun., 10, 4584, https://doi.org/10.1038/s41467-019-12541-7, 2019.
636 Ying, Q., Poulter, B., Watts, J. D., Arndt, K. A., Virkkala, A.-M., Bruhwiler, L., Oh, Y., Rogers, B. M., Natali, S. M., Sullivan,
637 H., Armstrong, A., Ward, E. J., Schiferl, L. D., Elder, C. D., Peltola, O., Bartsch, A., Desai, A. R., Euskirchen, E., Göckede,
638 M., Lehner, B., Nilsson, M. B., Peichl, M., Sonnentag, O., Tuittila, E.-S., Sachs, T., Kalhori, A., Ueyama, M., and Zhang, Z.:
639 $WetCH_4$: a machine-learning-based upscaling of methane fluxes of northern wetlands during 2016–2022, Earth Syst. Sci. Data,
640 17, 2507–2534, https://doi.org/10.5194/essd-17-2507-2025, 2025.

Yuan, K., Li, F., McNicol, G., Chen, M., Hoyt, A., Knox, S., Riley, W. J., Jackson, R., and Zhu, Q.: Boreal–Arctic wetland methane emissions modulated by warming and vegetation activity, Nat. Clim. Chang., 14, 282–288, https://doi.org/10.1038/s41558-024-01933-3, 2024.

Zhang, Z., Poulter, B., Melton, J. R., Riley, W. J., Allen, G. H., Beerling, D. J., Bousquet, P., Canadell, J. G., Fluet-Chouinard, E., Ciais, P., Gedney, N., Hopcroft, P. O., Ito, A., Jackson, R. B., Jain, A. K., Jensen, K., Joos, F., Kleinen, T., Knox, S. H., Li, T., Li, X., Liu, X., McDonald, K., McNicol, G., Miller, P. A., Müller, J., Patra, P. K., Peng, C., Peng, S., Qin, Z., Riggs, R. M., Saunois, M., Sun, Q., Tian, H., Xu, X., Yao, Y., Xi, Y., Zhang, W., Zhu, Q., Zhu, Q., and Zhuang, Q.: Ensemble estimates of global wetland methane emissions over 2000–2020, Biogeosciences, 22, 305–321, https://doi.org/10.5194/bg-22-305-2025, 2025.